Strong-coupling superconductivity in LiB_2C_2 trilayer films

Miao Gao [1,2,*] Xun-Wang Yan [3] Zhong-Yi Lu [4] and Tao Xiang [5,6]

[1]*Department of Microelectronics Science and Engineering, School of Physical Science and Technology, Ningbo University, Zhejiang 315211, China*

[2]*Laboratory of Clean Energy Storage and Conversion, Ningbo University, Zhejiang 315211, China*

[3]*College of Physics and Engineering, Qufu Normal University, Shandong 273165, China*

[4]*Department of Physics, Renmin University of China, Beijing 100872, China*

[5]*Institute of Physics, Chinese Academy of Sciences, Beijing 100190, China*

[6]*School of Physical Sciences, University of Chinese Academy of Sciences, Beijing 100049, China*

(Received 2 December 2019; revised manuscript received 2 February 2020; accepted 19 February 2020; published 2 March 2020)

Coupling between σ-bonding electrons and phonons is generally very strong. To metallize σ electrons provides a promising route to hunt for new high-T_c superconductors. Based on this picture and first-principles density functional calculation with Wannier interpolation for electronic structure and lattice dynamics, we predict that trilayer film LiB_2C_2 is a good candidate to realize this kind of high-T_c superconductivity. By solving the anisotropic Eliashberg equations, we find that free-standing trilayer LiB_2C_2 is a phonon-mediated superconductor with T_c exceeding the liquid-nitrogen temperature at ambient pressure. The transition temperature can be further raised to 125 K by applying a biaxial tensile strain.

DOI: 10.1103/PhysRevB.101.094501

I. INTRODUCTION

Boosting superconducting transition temperature, T_c, is one of the most important goals in the study of high-T_c superconductivity. According to Bardeen-Cooper-Schrieffer (BCS) theory [1], large density of states (DOS) at the Fermi level, strong electron-phonon coupling (EPC), and high-frequency phonons are beneficial for superconductivity. These three conditions are simultaneously fulfilled in MgB_2, whereas the coupling between metallic covalent σ bands and bond-stretching boron phonons play an essential role in its 39 K superconductivity [2–7]. Recently, Q carbon by substituting borons for 27% carbons was successfully synthesized [8]. This compound shows 55 K superconductivity at ambient pressure, breaking the record of T_c set by MgB_2, for purely phonon-mediated superconductors [8].

To search for new phonon-mediated superconductors with higher T_c at ambient pressure, a number of candidates have been suggested. Among them, quasi-two-dimensional compounds composed of Li, B, and C have been studied most intensively. The parent compound of these materials, LiBC [see Fig. 1(a)], is a semiconductor, which is isostructural and isovalent to MgB_2 [9,10]. By introducing vacancies at Li sites, Rosner *et al.* suggested that the covalent σ bands of LiBC will be partially occupied and become superconducting at about 100 K [11]. A similar prediction was made by Dewhurst *et al.* for $Li_{0.125}BC$ [12]. However, no evidence of superconductivity was reported down to 2 K in Li-deficient LiBC, i.e., Li_xBC, [13–16], due to dramatic structural distortions to the boron-carbon layers introduced by Li vacancies, which impedes the metallization of σ-bonding electrons [17].

Thus an unabridged Li lattice is important in stabilizing the crystal structure. In order to dope holes without introducing lattice distortion, replacing partially carbons by borons was proposed [18,19]. In particular, based on first-principles calculations, we predicted that both $Li_3B_4C_2$ and Li_2B_3C could become superconducting above 50 K [19]. A similar compound $Li_4B_5C_3$ was also predicted to be a superconductor at 16.8 K [20]. However, to synthesize these B-enriched stoichiometric compounds is difficult [21]. Experimentally, it was reported that hole-doped $Li_xB_{1.15}C_{0.85}$ shows a drastic decrease in resistivity below 20 K but remains nonsuperconducting [22].

Besides doping holes, applying pressure is another way to metallize LiBC. It was found that the crystal structure of LiBC remains unchanged up to 60 GPa [23]. Theoretically, the metallization occurs at a calculated pressure of 345 GPa, but the covalent σ bands remain unconducting [23]. By utilizing particle swarm optimization technique, Zhang uncovered a first-order phase transition for LiBC from the low-pressure to a high-pressure insulating phase, at about 108 GPa [24]. This transition is accompanied by the formation of sp^3-like boron-carbon networks. Thus, high pressure still cannot metallize the covalent σ bands of LiBC effectively.

Is it possible to find a metallic LiBC-like compound which is relatively simple to synthesize? In this work, we point out that a trilayer LiB_2C_2 film, which contains two honeycomb boron-carbon sheets intercalated by a vacancy-free triangular Li layer [Fig. 1], is just such a candidate. As no vacancies or substitutions are involved in trilayer LiB_2C_2, the holonomic Li lattice can inhibit the structural distortion in boron-carbon sheet. Furthermore, trilayer LiB_2C_2 is directly derived from bulk LiBC; it has a high probability to be successfully grown.

*gaomiao@nbu.edu.cn

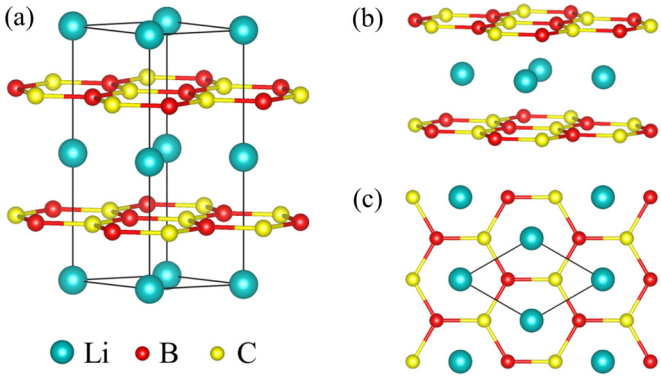

FIG. 1. Crystal structure of bulk LiBC (a) and that of trilayer LiB_2C_2 (b). (c) Top view of trilayer LiB_2C_2. The black line denotes the unit cell.

We have carried out first-principles calculation in conjunction with the Wannier interpolation technique to determine the electronic structure, lattice dynamics, and EPC for trilayer LiB_2C_2. We find that both σ and π bands emerge at the Fermi level in this two-dimensional material. The bond-stretching E_u and E_g phonon modes couple strongly with the metallized σ electrons. After solving the anisotropic Eliashberg equations, we find that the free-standing trilayer LiB_2C_2 is a two-gap superconductor, with T_c about 92 K. The superconducting temperature is enhanced by applying a biaxial tensile strain (BTS) to the film. The optimal BTS appears around 6–8%, at which the transition temperature could even reach 125 K. This enhancement can be understood by the increase of density of states (DOS) at the Fermi level and the strong softening relevant phonon modes under BTS.

II. COMPUTATIONAL METHODS

In our calculations, the plane wave basis method, as implemented in the QUANTUM ESPRESSO package [25], was adopted. We employed the generalized gradient approximation (GGA) of Perdew-Burke-Ernzerhof formula for the exchange-correlation potentials [26]. The optimized norm-conserving Vanderbilt pseudopotentials were used to model the electron-ion interactions [27,28]. After full convergence test, the kinetic energy cutoff and the charge density cutoff were set to 80 Ry and 320 Ry, respectively. The charge densities were determined self-consistently on an unshifted mesh of $40 \times 40 \times 1$ points with a Methfessel-Paxton smearing [29] of 0.02 Ry. The dynamical matrices and the perturbation potentials were calculated on a Γ-centered mesh of $10 \times 10 \times 1$ points, within the framework of density-functional perturbation theory [30].

The maximally localized Wannier functions (MLWFs) [31–33] were constructed on a $10 \times 10 \times 1$ grid of the Brillouin zone. We used eight Wannier functions to describe the band structure of trilayer LiB_2C_2 around the Fermi level. More specifically, two are p_z-like states of carbon atoms; six are σ-like states localized in the middle of boron-carbon bonds. The average spatial spread of the six σ-like states is just about 0.82 Å^2, showing excellent localization in space. With recently developed EPW code [34–36], the convergence of EPC constant λ was tested by electron mesh of $400 \times 400 \times 1$ points and phonon mesh of $200 \times 200 \times 1$ points. The Dirac δ functions for electrons and phonons were smeared out by a Gaussian function with the widths of 50 meV and 0.5 meV, respectively. Two affordable meshes ($300 \times 300 \times 1$ for electrons and $100 \times 100 \times 1$ for phonons) were adopted to solve the anisotropic Eliashberg equations to determine the superconducting properties of trilayer LiB_2C_2.

The anisotropic Eliashberg equations are composed of the superconducting gap $\Delta_{n\mathbf{k}}(i\omega_j)$ and the renormalization function $Z_{n\mathbf{k}}(i\omega_j)$, which read [36–38]

$$Z_{n\mathbf{k}}(i\omega_j) = 1 + \frac{\pi T}{N(0)\omega_j} \sum_{m\mathbf{k}'j'} \frac{\omega_{j'}}{\sqrt{\omega_{j'}^2 + \Delta_{m\mathbf{k}'}^2(i\omega_{j'})}} \times \lambda(n\mathbf{k}, m\mathbf{k}', \omega_j - \omega_{j'})\delta(\epsilon_{m\mathbf{k}'}), \quad (1)$$

and

$$Z_{n\mathbf{k}}(i\omega_j)\Delta_{n\mathbf{k}}(i\omega_j) = \frac{\pi T}{N(0)} \sum_{m\mathbf{k}'j'} \frac{\Delta_{m\mathbf{k}'}(i\omega_{j'})}{\sqrt{\omega_{j'}^2 + \Delta_{m\mathbf{k}'}^2(i\omega_{j'})}} \times [\lambda(n\mathbf{k}, m\mathbf{k}', \omega_j - \omega_{j'}) - \mu_c^*]\delta(\epsilon_{m\mathbf{k}'}). \quad (2)$$

The Matsubara frequencies are denoted by $i\omega_j = i(2j+1)\pi T$, with j being an integer. T is the absolute temperature. $\epsilon_{n\mathbf{k}}$ and $\epsilon_{m\mathbf{k}'}$ are the eigenvalues of the Kohn-Sham states $n\mathbf{k}$ and $m\mathbf{k}'$ with respect to the Fermi level. $N(0)$ is the DOS per spin at the Fermi level. μ_c^* describes the Coulomb pseudopotential, whose value is generally taken to be between 0.1 and 0.2.

$\lambda(n\mathbf{k}, m\mathbf{k}', \omega_j - \omega_{j'})$ measures the anisotropic EPC strength

$$\int_0^\infty d\omega \frac{2\omega}{(\omega_j - \omega_{j'})^2 + \omega^2} \alpha^2F(n\mathbf{k}, m\mathbf{k}', \omega), \quad (3)$$

in which $\alpha^2F(n\mathbf{k}, m\mathbf{k}', \omega)$ is the momentum-resolved Eliashberg spectral function.

$$\alpha^2F(n\mathbf{k}, m\mathbf{k}', \omega) = N(0) \sum_\nu |g_\nu(n\mathbf{k}, m\mathbf{k}')|^2 \delta(\omega - \omega_{\mathbf{q}\nu}). \quad (4)$$

Here $\mathbf{q}$ and ν stand for the wave vector and branch index of a phonon, and $\mathbf{q}$ is equal to $\mathbf{k}' - \mathbf{k}$. $g_\nu(n\mathbf{k}, m\mathbf{k}')$ denotes the EPC matrix element.

When numerically solving the imaginary-axis anisotropic Eliashberg equations, it is necessary to truncate the sum over Matsubara frequencies. In our calculations, the number of frequency grid points was chosen to be 200. This means that we adopted different frequency cutoff (ω_c) for each temperature. For instance, ω_c corresponds to 1.1 eV at 10 K, about eight times the largest phonon frequency of free-standing trilayer LiB_2C_2. At 90 K, ω_c is equal to 9.8 eV, which is critical to obtain the convergent distribution of superconducting gap on the Fermi surface. The highest temperature with nonvanished gap defines the T_c.

Through summation over electronic states $n\mathbf{k}$ and $m\mathbf{k}'$, we can obtain the isotropic Eliashberg spectral function.

$$\alpha^2F(\omega) = \frac{1}{N(0)^2} \sum_{n\mathbf{k},m\mathbf{k}'} \alpha^2F(n\mathbf{k}, m\mathbf{k}', \omega)\delta(\epsilon_{n\mathbf{k}})\delta(\epsilon_{m\mathbf{k}'}) \quad (5)$$

The total EPC constant λ can be calculated through

$$\lambda = \sum_{\mathbf{q}\nu} \lambda_{\mathbf{q}\nu} = 2 \int \frac{\alpha^2F(\omega)}{\omega} d\omega. \quad (6)$$

$\lambda_{\mathbf{q}\nu}$ is the momentum-dependent EPC constant, with which we can identify the strongly coupled phonon modes.

$$\lambda_{\mathbf{q}\nu} = \frac{2}{N(0)} \sum_{nm\mathbf{k}} \frac{1}{\omega_{\mathbf{q}\nu}} |g_\nu(n\mathbf{k}, m\mathbf{k}')|^2 \delta(\epsilon_{n\mathbf{k}}) \delta(\epsilon_{m\mathbf{k}'}). \quad (7)$$

When calculating the cleaved LiBC(0001) surface, a 2×2 supercell in the *ab* plane was employed, if we regarded the initial in-plane cell of LiBC as 1×1. Three different slab models were used to determine the stable surface structure. The terminated surfaces for these three models are unabridged Li layer (ULL), half Li with uniform distribution (HLU), and BC layer (BCL), respectively. Inversion symmetry is maintained for all the slabs. After cleaving bulk LiBC, we can obtain two HLU surfaces, or one ULL surface plus one BCL surface. By comparing their energies, we will find the more favorable surface structure. The thickness of these slabs along the *c* axis was set to 50 Å. For the half-Li-covered slab, there are eight BC sheets and seven unabridged Li layers inside the outmost surface Li.

As a comparison, we also calculated the exfoliation energy of graphene. The cells for bulk graphite were relaxed with semiempirical van der Waals correction [39,40]. The optimized lattice constants for graphite along the *a* and *c* axes are found to be 2.459 Å and 6.408 Å, consistent with experiment [41]. With these parameters, we constructed a slab model to represent the (0001) surface of graphite, with *c*-axis thickness also being 50 Å. There are totally eleven carbon sheets in the slab before exfoliating graphene. The exfoliation energy for graphene was calculated to be 0.023 eV/Å^2, in excellent agreement with existing data [42,43].

III. RESULTS AND ANALYSIS

In LiBC, Li atoms occupy the interstitial sites of layered honeycomb boron-carbon sheets [Fig. 1(a)]. The optimized lattice constants of bulk LiBC, obtained from our calculations, are 2.743 Å and 7.029 Å along the *a* and *c* axes, in good agreement with the experimental results ($a = 2.752$ Å and $c = 7.058$ Å) [9]. Trilayer LiB_2C_2 is built from the middle three layers of bulk LiBC [Fig. 1(b)]. The *c*-axis lattice parameter of the slab model for this trilayer LiB_2C_2 was set to 15 Å to avoid unphysical interactions between *c*-axis replicas. The in-plane lattice constant of trilayer LiB_2C_2 is 2.706 Å, slightly smaller than in the bulk. Boron atom moves outward by 0.054 Å with respect to the location of carbon atom, forming a buckled layer with carbons.

Figure 2 shows the band structure, DOS, and Fermi surfaces of trilayer LiB_2C_2. The σ bands are partially filled [Fig. 2(a)]. The π (bonding) and π^* (antibonding) bands formed by p_z orbitals of carbon and boron atoms are separated by a direct energy gap of 2.1 eV. Two Dirac-cone states at the *K* point are observed. In comparison with the B-p_z orbital, the C-p_z orbital has larger contribution to the π bands [Fig. 2(b)], due to its lower on-site energy. There are four bands across the Fermi level. The Fermi surface sheets, represented by the two circles [Figs. 2(c) and 2(d)] and two hexagons [Figs. 2(e) and 2(f)] surrounding the Γ point, are contributed mainly by σ electrons. The pockets at the Brillouin-zone corners [Fig. 2(e)] and the bigger circle [Fig. 2(f)] are associated with the π bands. The DOS at the Fermi level of trilayer LiB_2C_2 (Table I) is almost twice that of MgB_2 [4].

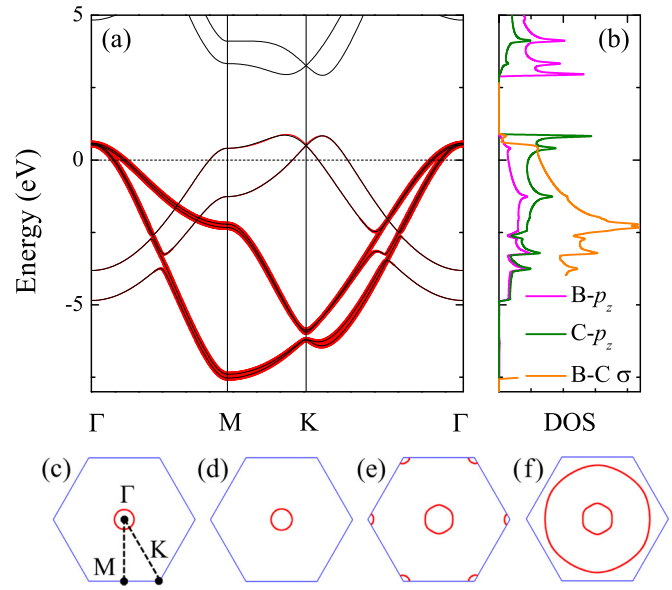

FIG. 2. Electronic structure of trilayer LiB_2C_2. (a) Band structure. The width of the red line is proportional to the weight of sp^2-hybridized σ orbitals in that band. The Fermi energy was set to zero. (b) Orbital-resolved DOS. (c)–(f) Fermi surfaces.

Figure 3 shows the $\lambda_{\mathbf{q}\nu}$-weighted phonon spectrum and vibrational patterns of strongly coupled phonon modes in trilayer LiB_2C_2. The free-standing trilayer LiB_2C_2 is dynamically stable because there is no imaginary frequency in the phonon spectrum [Fig. 3(a)]. The two strongly coupled phonon modes, E_u and E_g, only involve the in-plane vibrations of boron and carbon atoms [Figs. 3(b) and 3(c)]. The frequencies of E_u and E_g modes are respectively 85.16 meV and 87.68 meV at the Γ point, about 20.3% and 23.8% higher than that of E_{2g} modes in MgB_2 [44]. This can be attributed to the stronger boron-carbon σ bonds and larger interatomic force constants in trilayer LiB_2C_2. Besides these two modes, several low-frequency phonon modes have also sizable contribution to $\lambda_{\mathbf{q}\nu}$.

Figure 4 shows the isotropic Eliashberg spectral function $\alpha^2F(\omega)$, total and projected phonon DOS. The main peak of $\alpha^2F(\omega)$ around 87 meV results from the E_u and E_g modes. From the projected phonon DOS calculated through quasiharmonic approximation [Figs. 3(b) and 3(c)], it is clear that the low-frequency phonon DOS is contributed mainly by the out-of-plane displacements of boron and carbon atoms. These modes become more active in EPC due to the removal of quantum confinement [45,46]. A sharp peak of $F(\omega)$ surrounding 50 meV is contributed by Li phonons. However, $\alpha^2F(\omega)$ is insignificant near 50 meV, indicating that the coupling between electrons and Li phonons is rather weak. The EPC constant λ of free-standing trilayer LiB_2C_2 is 1.25, about 67.1% higher than that of MgB_2 [38,47,48].

Figure 5 shows the distribution of superconducting energy gaps $\Delta_{n\mathbf{k}}$ and $\lambda_{n\mathbf{k}}$ on the Fermi surface. There are two anisotropic superconducting gaps, associated with the σ bands and the π bands [Fig. 5(a)], respectively. The highest

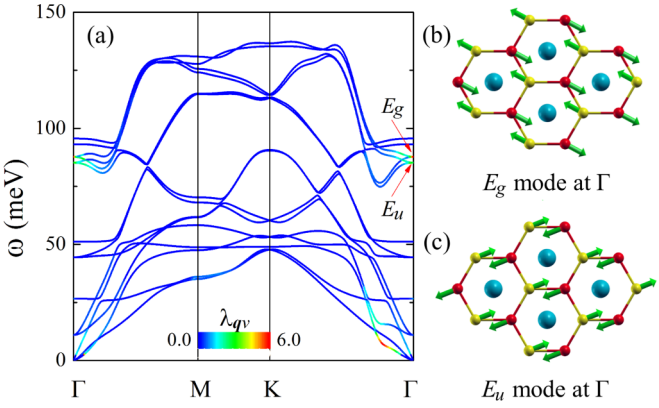

FIG. 3. (a) Phonon spectrum of trilayer LiB_2C_2 with a color representation of $\lambda_{\mathbf{q}v}$ at given wave vectors and modes. The vibrational patterns for strongly coupled (b) E_u and (c) E_g phonon modes. The direction and relative amplitude of atomic movement were represented by green arrows and their lengths, respectively.

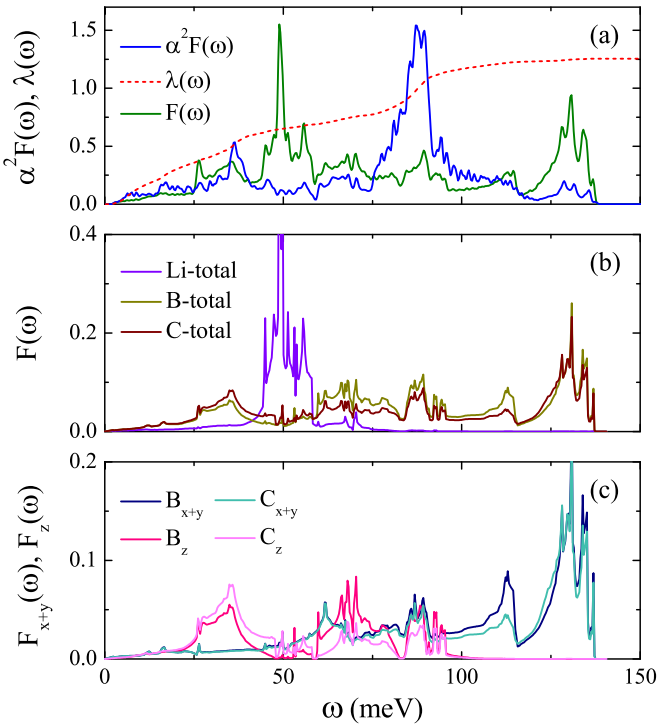

FIG. 4. (a) Eliashberg spectral function $\alpha^2F(\omega)$, phonon DOS $F(\omega)$, and accumulated $\lambda(\omega)$ for trilayer LiB_2C_2. (b) Projected phonon DOS. (c) In-plane and out-of-plane decompositions of boron and carbon phonon DOS.

temperature with nonvanished gap is about 92 K, corresponding to T_c [Fig. 5(c)]. The two-gap superconductivity results from the anisotropy of EPC constant $\lambda_{n\mathbf{k}}$ on different Fermi sheets [Fig. 5(b)]. The σ electrons, especially those around the inner pocket shown in Fig. 5(b), couple strongly with the E_u and E_g modes. The Fermi-surface averaged gaps are $\Delta_\sigma = 17.3$ meV and $\Delta_\pi = 4.7$ meV at 10 K. The anisotropy of Δ_σ is slightly stronger than that of Δ_π [Fig. 5(c)]. In MgB_2, the measured Δ_σ and Δ_π at 4.2 K are in the ranges of 7.0–7.1 meV and 2.3–2.8 meV [49–51], respectively. Δ_σ of trilayer LiB_2C_2 is about 2.47 times that of MgB_2.

To further raise T_c, we apply a BTS, described by $\epsilon = (a - a_0)/a_0 \times 100\%$, to trilayer LiB_2C_2. Here a_0 and a are the in-plane lattice constants before and after BTS. The boron-carbon sheet becomes more and more flat with the increase of BTS, and the separation between two layers is gradually depressed (Table I). These structural changes have significant impacts on the band structure of trilayer LiB_2C_2. On one hand, the p_z orbital experiences an enhanced Coulomb repulsion from the Li layer. As a consequence, the energies of π bands are increased. The valence bands near the Γ point shrink below the Fermi level, but the energy of Dirac point is almost unaffected with respect to the Fermi level. On the other hand, BTS reduces the overlap among atomic orbitals and weakens the dispersion of energy bands, enlarging the electronic DOS at the Fermi level. Above 12% BTS, there is a sudden abatement in the σ-band DOS at the Fermi level, $N_\sigma(0)$, due to almost complete occupation of two σ bands (Table I).

TABLE I. Calculated lattice parameter, electronic structure, EPC properties, and T_c for trilayer LiB_2C_2 under BTS. h_C represents the height of carbon atom from the Li layer. h_B-h_C is the buckling height of the boron-carbon sheet. $N_\sigma(0)$ and $N_\pi(0)$ denote the σ-band and π-band DOS at the Fermi level, respectively. $E_{\sigma_1\Gamma}$ and $E_{\sigma_2\Gamma}$ stand for the energies of valance bands at the Γ point. The frequencies of strongly coupled phonon modes are labeled by ω_{E_u} and ω_{E_g}. $\omega_{\log}$ and $\langle\omega^2\rangle$ can be determined through $\exp[\frac{2}{\lambda}\int\frac{d\omega}{\omega}\alpha^2F(\omega)\ln\omega]$ and $\frac{2}{\lambda}\int d\omega\alpha^2F(\omega)\omega$. $T_{c,0.1}^{\text{Aniso}}$ and $T_{c,0.2}^{\text{Aniso}}$ are T_cs determined by solving the anisotropic Eliashberg equations, when setting the Coulomb pseudopotential μ_c^* to 0.1 and 0.2. $T_{c,0.1}^{\text{MAD}}$ stands for T_c evaluated by the semiempirical McMillian-Allen-Dynes formula [57] with μ_c^* of 0.1. The units for height, DOS, energy, frequency, and T_c are Å, states spin^{-1} eV^{-1} cell^{-1}, eV, meV, and K, respectively.

ϵ	h_C	h_B-h_C	$N(0)$	$N_\sigma(0)$	$N_\pi(0)$	$E_{\sigma_1\Gamma}$	$E_{\sigma_2\Gamma}$	ω_{E_u}	ω_{E_g}	λ	$\omega_{\log}$	$\sqrt{\langle\omega^2\rangle}$	$T_{c,0.1}^{\text{MAD}}$	$T_{c,0.1}^{\text{Aniso}}$	$T_{c,0.2}^{\text{Aniso}}$
0	1.721	0.054	0.602	0.319	0.282	0.527	0.578	85.16	87.68	1.25	38.60	63.37	42.3	92	82
2	1.710	0.050	0.613	0.323	0.290	0.420	0.479	69.14	72.43	1.19	46.57	63.26	47.8	102	95
4	1.696	0.048	0.624	0.326	0.298	0.317	0.386	52.25	56.62	1.30	49.15	58.91	55.9	115	108
6	1.680	0.045	0.634	0.328	0.306	0.218	0.298	36.22	42.52	1.60	44.59	51.68	70.9	125	119
8	1.661	0.043	0.643	0.330	0.312	0.121	0.214	32.87	39.80	1.52	47.62	51.99	71.0	125	120
10	1.639	0.041	0.624	0.306	0.318	0.022	0.133	47.95	51.80	0.95	52.42	59.24	39.3	102	97
12	1.618	0.040	0.493	0.171	0.323	−0.097	0.033	70.01	71.10	0.41	47.15	63.39	2.5		
14	1.604	0.038	0.336	0.010	0.326	−0.247	−0.101	84.21	84.06	0.30	43.70	53.35	0.2		[a]

[a]When the EPC is weak, it is very difficult to ascertain the exact value of T_c for trilayer LiB_2C_2 at low temperature due to prohibitive computational cost.

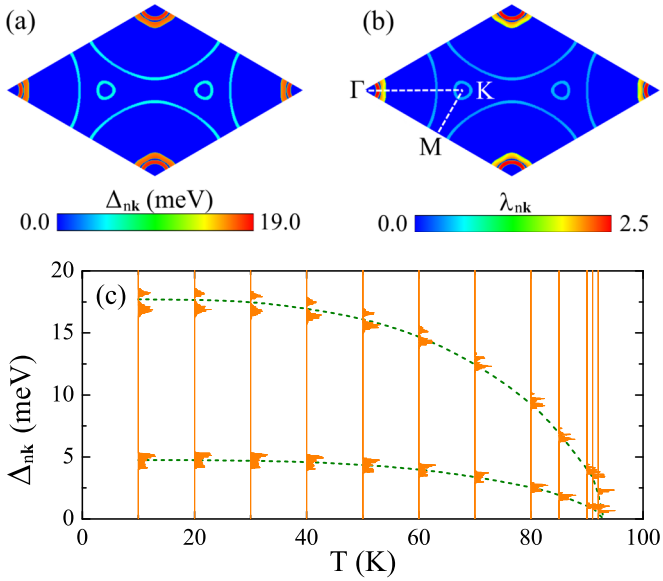

FIG. 5. (a) Distribution of superconducting gap $\Delta_{n\mathbf{k}}$ on the Fermi surface at 10 K. (b) The momentum-resolved EPC strength $\lambda_{n\mathbf{k}}$ for each electronic state n**k** on the Fermi surface. Here $\lambda_{n\mathbf{k}}$ is computed through $\sum_{m\mathbf{k}'} \lambda(n\mathbf{k}, m\mathbf{k}', 0)\delta(\epsilon_{m\mathbf{k}'})/N(0)$ [38]. For convenience, these two figures were drawn in the reciprocal unit cell. Electronic state n**k**, whose energy lies within ±0.1 eV from the Fermi level, are included in the calculation. (c) Temperature dependence of the gap values $\Delta_{n\mathbf{k}}$ on the Fermi surface at different temperatures.

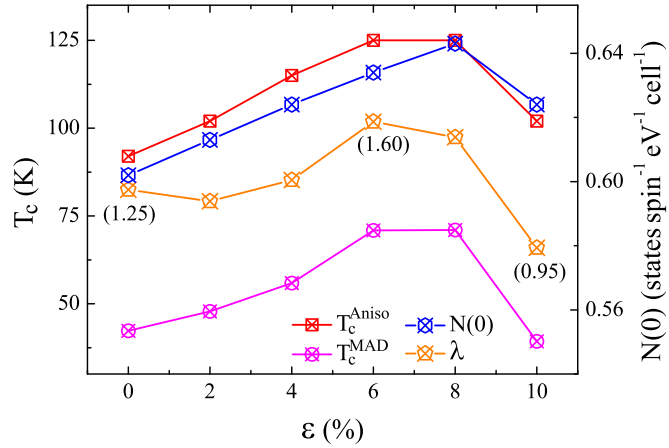

FIG. 6. The T_c, $N(0)$, and λ of trilayer LiB_2C_2 under BTS. The T_c obtained by the McMillian-Allen-Dynes formula is also given for comparison.

With the increase of BTS, the strongly coupled phonon modes become softened (Table I), and the EPC constant λ is increased. Compared with the strain-free case, λ increases by 28.0% under 6% BTS. Moreover, trilayer LiB_2C_2 is rather stable against BTS. No imaginary phonon frequency is found up to 8% BTS. A tiny imaginary phonon frequency of $1.97i$ meV emerges only when BTS is above 14%. Even this imaginary frequency may not be a signature of lattice instability, because similar phenomenon was also found in the simulations of germanene [52], β_{12} borophene [53], buckled arsenene [54,55]. This phenomenon may result from numerical difficulties in determining rapid decayed interatomic forces [56]. Above 10% BTS, there are abnormal arises of phonon frequencies for the E_u and E_g modes (Table I), probably related to the decline of $N_\sigma(0)$ [44,46].

Figure 6 shows the BTS dependence of T_c, determined by self-consistently solving the anisotropic Eliashberg equations. A domelike structure is observed. The maximal T_c is about 125 K. For strained trilayer LiB_2C_2, the transition temperature is predominantly determined by the electronic DOS at the Fermi level and the EPC constant λ (Fig. 6).

Since mechanical exfoliation from the bulk phase is a robust method to produce ultraclean, highly crystalline thin films [58], we also examine the possibility of synthesizing trilayer LiB_2C_2 from LiBC. After cleaving the (0001) plane of LiBC, we find that the most favorable structure is a half-Li-terminated surface, with evenly distributed Li atoms. This can balance the chemical valence as uniformly as possible. A BC-sheet-terminated surface has a disadvantage in energy, about 0.092 eV/Å^2. So the film that we can obtain after exfoliation is not trilayer LiB_2C_2, but trilayer LiB_2C_2 with half-Li covering on each side. The exfoliation energy for half-Li-covered trilayer LiB_2C_2 is 0.142 eV/Å^2, about six times that of graphene [42,43]. The extra surface Li on trilayer LiB_2C_2 can be further removed, for example, through vertical manipulation of tip in scanning tunneling microscopy (STM) experiment [59]. We also calculate the formation energy of free-standing trilayer LiB_2C_2 with respect to body-centered cubic lithium, α-B_{12} [60], and graphite. It is found that the formation energy is about −20.7 meV/formula. This suggests that trilayer LiB_2C_2 can be synthesized under special condition.

IV. CONCLUSION

In summary, based on first-principles density functional calculation and Wannier interpolation, we show that the σ bands in trilayer LiB_2C_2 are partially occupied. These metallized σ electrons couple strongly with the E_u and E_g phonon modes, driving this material into a high-T_c superconducting phase at ambient pressure. Applying biaxial tensile strain to trilayer LiB_2C_2 can significantly boost the T_c to a higher temperature.

ACKNOWLEDGMENTS

M.G. thank E. R. Margine for her help in the calculation and W. Ji for useful discussion. This work was supported by the National Key R & D Program of China (Grant No. 2017YFA0302900), National Natural Science Foundation of China (Grants No. 11888101, No. 11774422, No. 11974194, and No. 11974207), and Zhejiang Provincial Natural Science Foundation of China (Grant No. LY17A040005). M.G. was also sponsored by K. C. Wong Magna Fund in Ningbo University.

[1] J. Bardeen, L. N. Cooper, and J. R. Schrieffer, Phys. Rev. **108**, 1175 (1957).

[2] J. Nagamatsu, N. Nakagawa, T. Muranaka, Y. Zenitani, and J. Akimitsu, Nature (London) **410**, 63 (2001).

[3] J. M. An and W. E. Pickett, Phys. Rev. Lett. **86**, 4366 (2001).
[4] Y. Kong, O. V. Dolgov, O. Jepsen, and O. K. Andersen, Phys. Rev. B **64**, 020501(R) (2001).
[5] T. Yildirim, O. Gülseren, J. W. Lynn, C. M. Brown, T. J. Udovic, Q. Huang, N. Rogado, K. A. Regan, M. A. Hayward, J. S. Slusky, T. He, M. K. Haas, P. Khalifah, K. Inumaru, and R. J. Cava, Phys. Rev. Lett. **87**, 037001 (2001).
[6] H. J. Choi, D. Roundy, H. Sun, M. L. Cohen, and S. G. Louie, Phys. Rev. B **66**, 020513(R) (2002).
[7] H. J. Choi, D. Roundy, H. Sun, M. L. Cohen, and S. G. Louie, Nature (London) **418**, 758 (2002).
[8] A. Bhaumik, R. Sachan, S. Gupta, and J. Narayan, ACS Nano **11**, 11915 (2017).
[9] M. Wörle, R. Nesper, G. Mair, M. Schwarz, and H. G. Vonschnering, Z. Anorg. Allg. Chem. **621**, 1153 (1995).
[10] P. F. Karimov, N. A. Skorikov, E. Z. Kurmaev, L. D. Finkelstein, S. Leitch, J. MacNaughton, A. Moewes, and T. Mori, J. Phys.: Condens. Matter **16**, 5137 (2004).
[11] H. Rosner, A. Kitaigorodsky, and W. E. Pickett, Phys. Rev. Lett. **88**, 127001 (2002).
[12] J. K. Dewhurst, S. Sharma, C. Ambrosch-Draxl, and B. Johansson, Phys. Rev. B **68**, 020504(R) (2003).
[13] A. Bharathi, S. J. Balaselvi, M. Premila, T. N. Sairam, G. L. N. Reddy, C. S. Sundar, and Y. Hariharan, Solid State Commun. **124**, 423 (2002).
[14] D. Souptela, Z. Hossainb, G. Behra, W. Lösera, and C. Geibel, Solid State Commun. **125**, 17 (2003).
[15] A. M. Fogg, P. R. Chalker, J. B. Claridge, G. R. Darling, and M. J. Rosseinsky, Phys. Rev. B **67**, 245106 (2003).
[16] A. M. Fogg, J. B. Claridge, G. R. Darling, and M. J. Rosseinsky, Chem. Commun. **12**, 1348 (2003).
[17] A. M. Fogg, J. Meldrum, G. R. Darling, J. B. Claridge, and M. J. Rosseinsky, J. Am. Chem. Soc. **128**, 10043 (2006).
[18] R. Miao, J. Yang, M. Jiang, Q. Zhang, D. Cai, C. Fan, Z. Bai, C. Liu, F. Wu, and S. Ma, J. Appl. Phys. **113**, 133910 (2013).
[19] M. Gao, Z.-Y. Lu, and T. Xiang, Phys. Rev. B **91**, 045132 (2015).
[20] T. Bazhirov, Y. Sakai, S. Saito, and M. L. Cohen, Phys. Rev. B **89**, 045136 (2014).
[21] V. Milashius, V. Pavlyuk, G. Dmytriv, and H. Ehrenberg, Inorg. Chem. Front **5**, 853 (2018).
[22] A. Noguchi, S. Emori, Y. Takahashi, K. Takase, T. Watanabe, K. Sekizawa, and Y. Takano, J. Phys.: Conf. Ser. **150**, 052188 (2009).
[23] A. Lazicki, C.-S. Yoo, H. Cynn, W. J. Evans, W. E. Pickett, J. Olamit, K. Liu, and Y. Ohishi, Phys. Rev. B **75**, 054507 (2007).
[24] M. Zhang, Europhys. Lett. **114**, 16001 (2016).
[25] P. Giannozzi, S. Baroni, N. Bonini, M. Calandra, R. Car, C. Cavazzoni, D. Ceresoli, G. L. Chiarotti, M. Cococcioni, I. Dabo, A. Dal Corso, S. de Gironcoli, S. Fabris, G. Fratesi, R. Gebauer, U. Gerstmann, C. Gougoussis, A. Kokalj, M. Lazzeri, L. Martin-Samos *et al.*, J. Phys.: Condens. Matter **21**, 395502 (2009).
[26] J. P. Perdew, K. Burke, and M. Ernzerhof, Phys. Rev. Lett. **77**, 3865 (1996).
[27] D. R. Hamann, Phys. Rev. B **88**, 085117 (2013).
[28] M. Schlipf and F. Gygi, Comput. Phys. Commun. **196**, 36 (2015).
[29] M. Methfessel and A. T. Paxton, Phys. Rev. B **40**, 3616 (1989).
[30] S. Baroni, S. de Gironcoli, A. Dal Corso, and P. Giannozzi, Rev. Mod. Phys. **73**, 515 (2001).
[31] N. Marzari and D. Vanderbilt, Phys. Rev. B **56**, 12847 (1997).
[32] I. Souza, N. Marzari, and D. Vanderbilt, Phys. Rev. B **65**, 035109 (2001).
[33] A. A. Mostofi, J. R. Yates, Y.-S. Lee, I. Souza, D. Vanderbilt, and N. Marzari, Comput. Phys. Commun. **178**, 685 (2008).
[34] F. Giustino, M. L. Cohen, and S. G. Louie, Phys. Rev. B **76**, 165108 (2007).
[35] J. Noffsinger, F. Giustino, B. D. Malone, C.-H. Park, S. G. Louie, and M. L. Cohen, Comput. Phys. Commun. **181**, 2140 (2010).
[36] S. Poncé, E. R. Margine, C. Verdi, and F. Giustino, Comput. Phys. Commun. **209**, 116 (2016).
[37] H. J. Choi, M. L. Cohen, and S. G. Louie, Physica C **385**, 66 (2003).
[38] E. R. Margine and F. Giustino, Phys. Rev. B **87**, 024505 (2013).
[39] S. Grimme, J. Comp. Chem. **27**, 1787 (2006).
[40] V. Barone, M. Casarin, D. Forrer, M. Pavone, M. Sambi, and A. Vittadini, J. Comp. Chem. **30**, 934 (2009).
[41] P. Trucano and R. Chen, Nature (London) **258**, 136 (1975).
[42] R. Zacharia, H. Ulbricht, and T. Hertel, Phys. Rev. B **69**, 155406 (2004).
[43] L. Spanu, S. Sorella, and G. Galli, Phys. Rev. Lett. **103**, 196401 (2009).
[44] K.-P. Bohnen, R. Heid, and B. Renker, Phys. Rev. Lett. **86**, 5771 (2001).
[45] G. Profeta, M. Calandra, and F. Mauri, Nat. Phys. **8**, 131 (2012).
[46] M. Gao, X.-W. Yan, J. Wang, Z.-Y. Lu, and T. Xiang, Phys. Rev. B **100**, 024503 (2019).
[47] A. Eiguren and C. Ambrosch-Draxl, Phys. Rev. B **78**, 045124 (2008).
[48] M. Calandra, G. Profeta, and F. Mauri, Phys. Rev. B **82**, 165111 (2010).
[49] M. Iavarone, G. Karapetrov, A. E. Koshelev, W. K. Kwok, G. W. Crabtree, D. G. Hinks, W. N. Kang, E.-M. Choi, H. J. Kim, H.-J. Kim, and S. I. Lee, Phys. Rev. Lett. **89**, 187002 (2002).
[50] P. Szabó, P. Samuely, J. Kačmarčík, T. Klein, J. Marcus, D. Fruchart, S. Miraglia, C. Marcenat, and A. G. M. Jansen, Phys. Rev. Lett. **87**, 137005 (2001).
[51] R. S. Gonnelli, D. Daghero, G. A. Ummarino, V. A. Stepanov, J. Jun, S. M. Kazakov, and J. Karpinski, Phys. Rev. Lett. **89**, 247004 (2002).
[52] S. Cahangirov, M. Topsakal, E. Aktürk, H. Şahin, and S. Ciraci, Phys. Rev. Lett. **102**, 236804 (2009).
[53] M. Gao, Q.-Z. Li, X.-W. Yan, and J. Wang, Phys. Rev. B **95**, 024505 (2017).
[54] C. Kamal and M. Ezawa, Phys. Rev. B **91**, 085423 (2015).
[55] X. Kong, M. Gao, X.-W. Yan, Z.-Y. Lu, and T. Xiang, Chin. Phys. B **27**, 046301 (2018).
[56] H. Şahin, S. Cahangirov, M. Topsakal, E. Bekaroglu, E. Akturk, R. T. Senger, and S. Ciraci, Phys. Rev. B **80**, 155453 (2009).
[57] P. B. Allen and R. C. Dynes, Phys. Rev. B **12**, 905 (1975).
[58] A. K. Geim and K. S. Novoselov, Nat. Mater. **6**, 183 (2007).
[59] S.-W. Hla, J. Vac. Sci. Tech. **23**, 1351 (2005).
[60] B. F. Decker and J. S. Kasper, Acta Crystallogr. **12**, 503 (1959).